CHAPTER FOURTEEN

Miscellaneous Weighted Residual Methods

In the previous chapters, with an exception of GPG, the finite element formulations are based on the Galerkin methods in which test functions are chosen to be the same as the trial functions. This is not required in the weighted residual methods.

Weighted residual methods other than the Galerkin methods include spectral element methods (SEM), least square methods (LSM), moment methods, or collocation methods, in which the test functions or weighting functions are not necessarily the same as the trial functions. In spectral element methods (SEM), polynomials in terms of nodal values of the variables are combined with special functions such as Chebyshev or Legendre polynomials. For least square methods, the test functions are constructed by the derivative of the residual with respect to the nodal values of the variables. Some arbitrary functions are chosen as test functions for the moment and collocation methods. Recently, the weighted residual concept has been used in meshless configurations, known as the finite point method (FPM), partition of unity method, meshless cloud method, or element-free method.

In the following sections, we shall describe a certain type of spectral element methods, least square methods, optimal control methods (OCM), and finite point methods (FPM). They are selected here for discussion because of their possible future potential for further developments.

14.1 SPECTRAL ELEMENT METHODS

The term "spectral" as used here implies a special function. Examples of such functions may be Chebyshev, Legendre, or Laguerre polynomials. These functions are expected to portray physical phenomena more realistically and precisely than other functions that have been discussed previously, leading to a greater solution accuracy. However, their applications are limited to simple geometries and simple boundary conditions.

The spectral element methods (SEM) represent a recent development as a combination of the classical spectral methods and finite element methods, thus the term "spectral element." The classical spectral methods resemble the classical method of weighted residuals.

In the classical spectral methods, trial and test functions are chosen such that they satisfy global boundary conditions. In the spectral element method, the trial and test functions are local and combined with isoparametric finite element functions as first

proposed by Patera [1984]. Applications of the spectral element methods to triangular finite elements were reported by Sherwin and Karniadakis [1995]. The basic idea, however, was employed earlier in the so-called *p*-version finite elements [Babuska, 1958]. Later extensions can be seen in the *h-p* methods [Oden et al., 1989] and the flowfield-dependent variation spectral element methods (FDV-SEM) [Yoon and Chung, 1996]. The classical spectral methods are well documented in the book by Canuto et al. [1987]. Here, in this section, we utilize the concept of the classical spectral methods and apply it to the finite element method in such a way that the accuracy and efficiency are realized with a reasonable compromise. The most important aspect of SEM as applied to the FDV scheme is to portray turbulent behavior in direct numerical simulation (DNS) calculations. This will allow direct numerical simulation to be more efficient in which turbulence models are no longer required, as indicated in Section 13.6.

In SEM formulations, we may use either Chebyshev polynomials or Legendre polynomials. Patera [1984] demonstrated the SEM formulation using Chebyshev polynomials. We illustrate the use of Legendre polynomials [Szabo and Babuska, 1991] as test functions in the following subsection.

14.1.1 SPECTRAL FUNCTIONS

In the traditional spectral methods, we use spectral functions that are normally provided by Chebyshev polynomials or Legendre polynomials. Either one of these polynomials can be used in the spectral element methods. Before we proceed to SEM, we briefly summarize the basic properties involved in the Chebyshev polynomials and Legendre polynomials.

Chebyshev Polynomials

The basic concept of the least squares approximations is used to derive the Chebyshev polynomials in which orthogonality properties are preserved. To this end, consider a polynomial $\Phi_r(x)$ of degree r in x such that

$$\int_{-1}^{1} W(x)\Phi_r(x)q_{r-1}(x)dx = 0 \tag{14.1.1}$$

where $W(x)$ is the weighting function

$$W(x) = \frac{1}{\sqrt{1-x^2}} \tag{14.1.2}$$

and $q_{r-1}(x)$ is an arbitrary polynomial of degree $r-1$ or less in x.

Let us now introduce the change in variables

$$x = \cos\,\theta \tag{14.1.3}$$

Substituting (14.1.3) into (14.1.2) and (14.1.1) yields

$$\int_{0}^{\pi} \Phi_r(\cos\theta)q_{r-1}(\cos\theta)d\theta = 0 \tag{14.1.4}$$

which is satisfied by

$$\int_0^{\pi} \Phi_r(\cos\theta)\cos k\theta d\theta = 0 \quad (k = 0, 1, \ldots, r-1) \tag{14.1.5}$$

with

$$\Phi_r(\cos\theta) = C_r \cos r\theta \tag{14.1.6}$$

It follows from (14.1.3) that

$$\Phi_r(x) = C_r \cos(r \cos^{-1} x) \tag{14.1.7}$$

are the required orthogonal polynomials with $C_r = 1$. These polynomials are known as Chebyshev polynomials, which possess the orthogonality property

$$\int_{-1}^{1} (1-x^2)^{-\frac{1}{2}} T_r(x) T_s(x) dx = 0 \quad (r \neq s) \tag{14.1.8}$$

$$T_{r+1}(x) = 2x T_r(x) - T_{r-1}(x) \tag{14.1.9}$$

$$T_o(x) = 1, \qquad T_1(x) = x \tag{14.1.10}$$

The orthogonal square factor γ_r is given by

$$\gamma_r = \int_{-1}^{1} (1-x^2)^{-\frac{1}{2}} T_r^2(x) dx = 0 \tag{14.1.11}$$

Since $x = \cos\theta$, $T_r(x) = \cos r\theta$, we have

$$\gamma_r = \int_0^{\pi} \cos^2 r\theta d\theta = \begin{cases} \pi, & r = 0 \\ \frac{\pi}{2}, & r \neq 0 \end{cases} \tag{14.1.12}$$

Thus, the nth degree least squares polynomial approximation to $f(x)$ in $(-1, 1)$, relevant to the weighting function $W(x) = (1-x^2)^{-\frac{1}{2}}$, is defined as

$$y(x) = \sum_{r=0}^{n} a_r T_r(x) \quad (-1 \leq x \leq 1) \tag{14.1.13}$$

The least squares approximations require that

$$\int_{-1}^{1} W(x)[f(x) - y(x)]^2 dx = \min \tag{14.1.14}$$

or

$$\frac{\partial}{\partial a_r} \int_{-1}^{1} W(x) \left[f(x) - \sum_{r=0}^{n} a_r T_r(x) \right]^2 dx = 0 \tag{14.1.15}$$

$$a_r \left[\int_{-1}^{1} W(x) T_r^2 dx \right] - \int_{-1}^{1} W(x) f(x) T_r(x) dx = 0 \tag{14.1.16}$$

with

$$a_k = \frac{\int_{-1}^{1} W(x) f(x) T_r(x) dx}{\int_{-1}^{1} W(x) T_r^2 dx}$$

$$a_0 = \frac{1}{\pi} \int_{-1}^{1} (1 - x^2)^{-\frac{1}{2}} f(x) dx$$

$$a_r = \frac{2}{\pi} \int_{-1}^{1} (1 - x^2)^{-\frac{1}{2}} f(x) Tr(x) dx \tag{14.1.17a}$$

or in general

$$a_r = \frac{2}{NC_r} \sum_{j=0}^{N} \frac{1}{c_j} f(x_j) T_r(x_j) \qquad \begin{cases} x_j = \cos \frac{j\pi}{N} & j = 0, \quad 1 \ldots \\ C_0 = C_N = 2, & C_r = 1 \end{cases}$$

which has all polynomials of degree n or less, the integrated weighted square error

$$\int_{-1}^{1} (1 - x^2)^{-\frac{1}{2}} [f(x) - y_n(x)]^2 dx \tag{14.1.17b}$$

is the least when $y_n(x)$ is identified with the right-hand side of (14.1.13).

In terms of the nondimensional variable $\xi = x/\Delta x$, the Chebyshev polynomials are summarized as follows:

$$T_n(\xi) = \cos n\theta, \quad \theta = \cos^{-1} \xi \quad -1 \le \xi \le 1$$

$$T_0(\xi) = \cos 0 = 1$$

$$T_1(\xi) = \cos(\cos^{-1} \xi) = \xi$$

$$\xi T_n(\xi) = \cos n\theta \cos \theta = \frac{1}{2}[\cos(n-1)\theta + \cos(n+1)\theta]$$

or

$$\xi T_n(\xi) = \frac{1}{2}[T_{n-1}(\xi) + T_{n+1}(\xi)]$$

thus, the general formula is given by

$$T_{n+1}(\xi) = 2\xi T_n(\xi) - T_{n-1}(\xi) \tag{14.1.18}$$

$$T_0(\xi) = 1$$

$$T_1(\xi) = \xi$$

$$T_2(\xi) = 2\xi^2 - 1$$

$$T_3(\xi) = 4\xi^3 - 3\xi$$

$$T_4(\xi) = 8\xi^4 - 8\xi^2 + 1$$

$$T_5(\xi) = 16\xi^5 - 20\xi^3 - 5\xi$$

$$\vdots$$

Similar developments are applied to other directions for 2-D and 3-D geometries, which will then be utilized through tensor products for applications to multidimensional

problems. Applications of the Chebyshev polynomials to a spectral element method will be shown in Section 22.6.4.

Legendre Polynomials

The Legendre polynomials are based on the orthogonal properties of the least square concept. To this end, we require a polynomial $\Phi_r(x)$ of degree r in x such that

$$\int_a^b W(x)\Phi_r(x)q_{r-1}(x)dx = 0 \tag{14.1.19}$$

where $W(x) = 1$ is used for the Legendre polynomial. Consider the notation

$$W(x)\Phi_r(x) = \frac{d^r u_r(x)}{dx^r} \tag{14.1.20}$$

Thus, it follows from (14.1.19) and (14.1.20) that

$$\int_a^b u_r^{(r)}(x)q_{r-1}(x)dx = 0 \tag{14.1.21}$$

Integrating by parts

$$\left[u_r^{(r-1)}q_{r-1} - u_r^{(r-2)}q'_{r-1} + \cdots + (-1)^{r-1}u_r q_{r-1}^{(r-1)}\right]_a^b = 0 \tag{14.1.22}$$

The requirement for the function $\Phi_r\ (x)$ defined by (14.1.20)

$$\Phi_r(x) = \frac{1}{W(x)}\frac{d^r u_r(x)}{dx^r} \tag{14.1.23}$$

be a polynomial of degree r implies that $u_r(x)$ must satisfy the differential equation

$$\frac{d^{r+1}}{dx^{r+1}}\left[\frac{1}{W(x)}\frac{d^r u_r(x)}{dx^r}\right] = 0 \tag{14.1.24}$$

in [a, b] with the $2r$ boundary conditions

$$\begin{aligned} u_r(a) = u'_r(a) = u''_r(a) = \cdots = u_r^{(r-1)}(a) = 0 \\ u_r(b) = u'_r(b) = u''_r(b) = \cdots = u_r^{(r-1)}(b) = 0 \end{aligned} \tag{14.1.25}$$

For the least squares approximation over an interval of finite length, it is convenient to suppose that a linear change in variables has transformed that interval into the interval $[-1, 1]$. With $W(x) = 1$, we obtain

$$\frac{d^{2r+1}u_r}{dx^{2r+1}} = 0 \tag{14.1.26}$$

Using the boundary conditions (14.1.15) for $(-1, 1)$

$$u_r = \lambda_r(x^2 - 1)^r \tag{14.1.27}$$

where λ_r is an arbitrary constant. Hence, from (14.1.23) it follows that the rth relevant orthogonal polynomial is of the form

$$\Phi_r(x) = \lambda_r \frac{d^r}{dx^r}(x^2 - 1)^r \tag{14.1.28}$$

with

$$\lambda_r = \frac{1}{2^r p!} \tag{14.1.29}$$

The polynomial obtained in this manner is the rth Legendre polynomial

$$L_r(x) = \frac{1}{2^r r!}\frac{d^r}{dx^r}(x^2-1)^r \tag{14.1.30}$$

From the orthogonal property it follows that

$$\int_{-1}^{1} L_r(x)L_s(x)dx = 0 \quad r \neq s \tag{14.1.31}$$

The value assigned to λ_r is such that $L_r(x) = 1$ and it is true that $|L_r(x)| \leq 1$ when $|x| \leq 1$. With the nondimensional variable, this gives

$$\begin{aligned}
L_0(\xi) &= 1\\
L_1(\xi) &= \xi\\
L_2(\xi) &= \frac{1}{2}(3\xi^2-1)\\
L_3(\xi) &= \frac{1}{2}(5\xi^3-3\xi)\\
L_4(\xi) &= \frac{1}{8}(35\xi^4-30\xi^2+3)\\
L_5(\xi) &= \frac{1}{8}(63\xi^5-70\xi^3-15\xi)\\
L_6(\xi) &= \frac{1}{16}(231\xi^6-315\xi^4+105\xi^2-5)\\
L_7(\xi) &= \frac{1}{16}(429\xi^7-693\xi^5+315\xi^3-35\xi)\\
&\vdots
\end{aligned}$$

The recurrence formula is given by

$$\begin{aligned}
L_r(\xi) &= \frac{1}{2^r r!}\frac{d^r}{d\xi^r}(\xi^2-1)^r\\
L_{r+1}(\xi) &= \frac{2r+1}{r+1}\xi L_r(\xi) - \frac{r}{r+1}L_{r-1}(\xi)
\end{aligned} \tag{14.1.32}$$

Applications of the Legendre polynomials to a spectral element method will be shown in the next section.

14.1.2 SPECTRAL ELEMENT FORMULATIONS BY LEGENDRE POLYNOMIALS

The most efficient approach toward multidimensional applications of the spectral element methods is to utilize the isoparametric elements (quadrilaterals for 2-D and hexahedrals for 3-D). Using a linear element with only corner nodes, but accepting as high a spectral degree of freedom as desired for the side and interior modes for 2-D

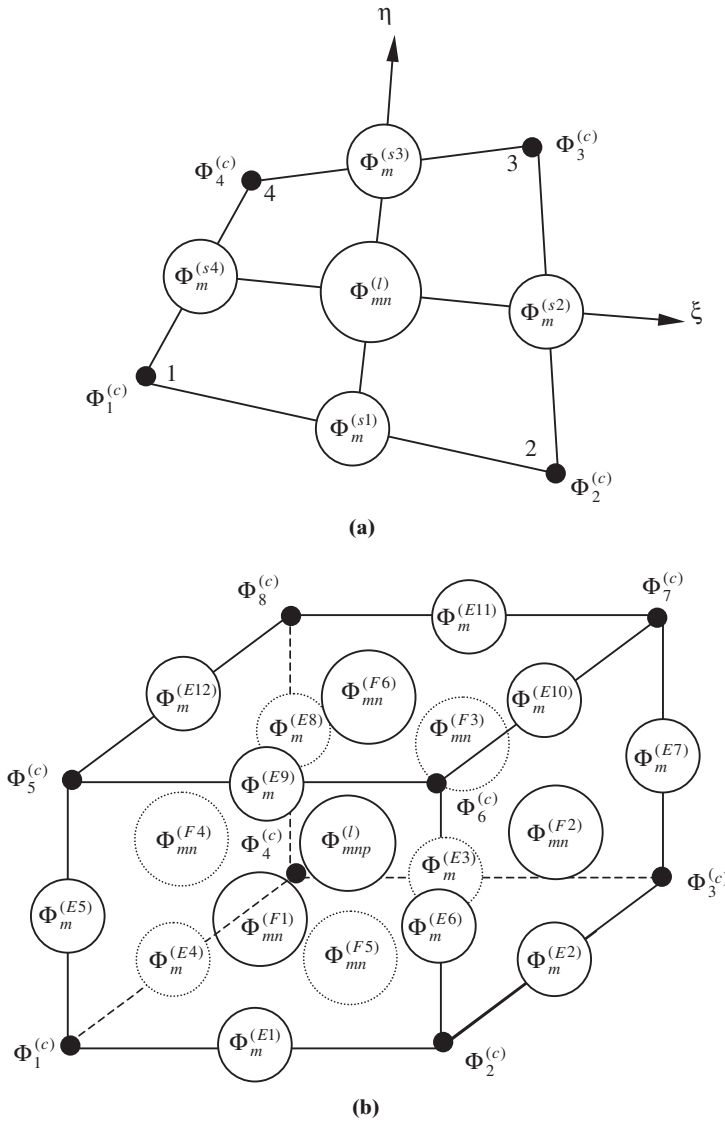

Figure 14.1.1 Spectral element configuration. **(a)** Two-dimensional spectral element. **(b)** Three-dimensional spectral element.

and the edge, face, and interior modes for 3-D, it is possible to construct Galerkin spectral element integrals. By means of static condensation, all spectral mode degrees of freedom are eliminated, resulting in the final algebraic equations only in terms of the corner nodes.

The spectral functions of the Legendre polynomials (14.1.32) are zero at the corner nodes but exhibit high order approximations elsewhere. In this process, any variable is to change nonlinearly everywhere but it is calculated only at the element corner nodes. To illustrate this point, let us consider the approximation of the variable **U**:

For two dimensions (Figure 14.1.1a) we have

Corner nodes: linear isoparametric function, $\Phi_N^{(c)}$

Side modes: Legendre spectral mode functions, $\Phi_m^{(s)}$
Interior modes: Legendre spectral mode functions, $\Phi_{mn}^{(I)}$

$$\mathbf{U} = \Phi_\alpha \mathbf{U}_\alpha + \Phi_m^{(s)} \hat{\mathbf{U}}_m + \Phi_{mn}^{(I)} \hat{\mathbf{U}}_{mn} \tag{14.1.33}$$

For three dimensions (Figure 14.1.1b) we have

Corner nodes: linear isoparametric function, $\Phi_N^{(c)}$
Edge modes: Legendre spectral mode functions, $\Phi_m^{(E)}$
Face modes: Legendre spectral mode functions, $\Phi_{mn}^{(F)}$
Interior modes: Legendre spectral mode functions, $\Phi_{mnp}^{(I)}$

$$\mathbf{U} = \Phi_\alpha \mathbf{U}_\alpha + \Phi_m^{(E)} \hat{\mathbf{U}}_m + \Phi_{mn}^{(F)} \hat{\mathbf{U}}_{mn} + \Phi_{mnp}^{(I)} \hat{\mathbf{U}}_{mnp} \tag{14.1.34}$$

where $\mathbf{U}_\alpha$ are the variables to be calculated at the corner nodes and $\hat{\mathbf{U}}_m$, $\hat{\mathbf{U}}_{mn}$, and $\hat{\mathbf{U}}_{mnp}$ denote spectral degrees of freedom.

The global trial functions Φ_α are assembled from the corner node linear isoparametric functions $\Phi_N^{(C)}$. The Legendre functions for the side modes $\Phi_m^{(s)}$ and the interior modes $\Phi_{mn}^{(I)}$ for two dimensions, and edge modes $\Phi_m^{(E)}$, face modes $\Phi_{mn}^{(F)}$, and interior modes $\Phi_{mnp}^{(I)}$ for three dimensions are given as follows:

For Two Dimensions

Side modes:

$$\begin{aligned}
\Phi_m^{(S1)} &= \frac{1}{2}(1-\eta)G_m(\xi) \\
\Phi_m^{(S2)} &= \frac{1}{2}(1+\xi)G_m(\eta) \\
\Phi_m^{(S3)} &= \frac{1}{2}(1+\eta)G_m(\xi) \\
\Phi_m^{(S4)} &= \frac{1}{2}(1-\xi)G_m(\eta)
\end{aligned} \tag{14.1.35}$$

with $m = 2, \ldots q$; $N^{(S)} = 4(q-1); q \geq 2$

Interior modes:

$$\Phi_{mn}^{(I)} = G_m(\xi)G_n(\eta) \tag{14.1.36}$$

with $m, n = 2, \ldots, q-2; (m+n) = 2, \ldots, q; N^{(I)} = \frac{1}{2}[(q-2)(q-3)], q \geq 4$

where $N^{(S)}$ and $N^{(I)}$ denote, respectively, the total number of functional modes available for sides (1, 2, 3, 4) and interior. The highest polynomial order chosen is denoted by q, and G_m refers to the Legendre polynomials defined as

$$G_m(\xi) = \frac{1}{\sqrt{2(2m-1)}}[L_m(\xi) - L_{m-2}(\xi)] \tag{14.1.37}$$

with the recursive formula given by

$$L_{m+1}(\xi) = \frac{2m+1}{m+1}\xi L_m(\xi) - \frac{m}{m+1}L_{m-1}(\xi) \tag{14.1.38}$$

Similar results are obtained for the η-direction. For illustration, variable orders of Legendre polynomials specified in different elements are shown in Figure 14.1.2. At

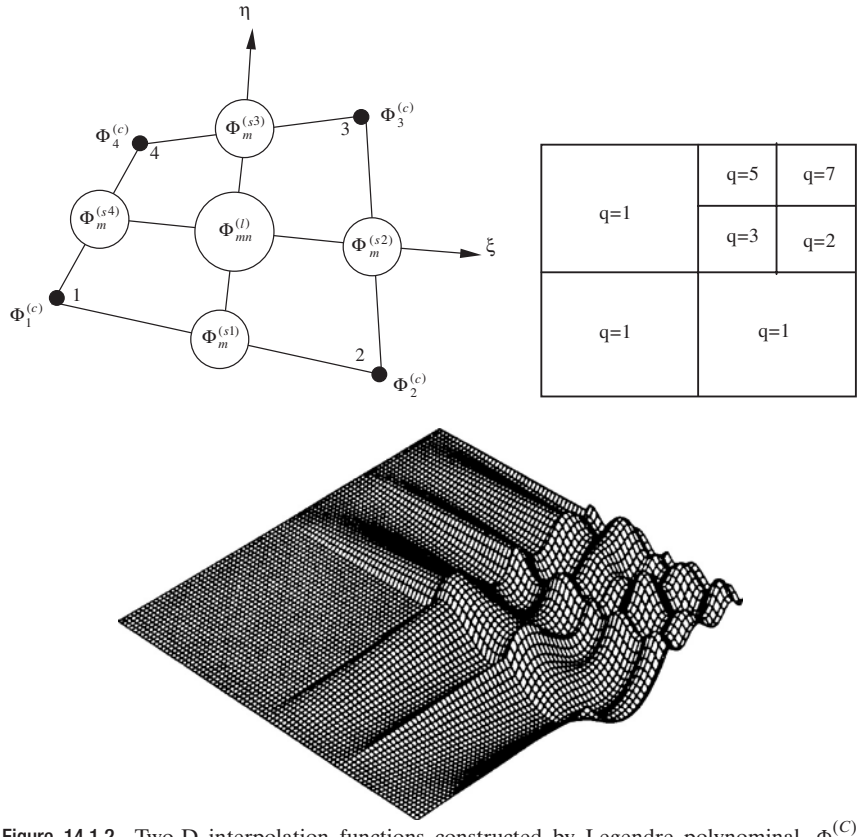

Figure 14.1.2 Two-D interpolation functions constructed by Legendre polynominal, $\Phi_N^{(C)}$ (corner nodes), $\Phi_M^{(S)}$ (side nodes), $\Phi_{mn}^{(1)}$ (interior nodes).

boundaries, higher order functions prevail over the lower order functions. In addition to the above polynomial space, (called $S1$) we may use another option of the space (called $S2$) in which $(q-1)^2$ interior modes are applied.

For Three Dimensions

$$\begin{aligned}\text{Edge mode:}\quad & \Phi_m^{(E1)} = \tfrac{1}{4}(1-\eta)(1-\zeta)G_m(\xi)\\ & \Phi_m^{(E2)} = \tfrac{1}{4}(1+\xi)(1-\zeta)G_m(\eta)\\ & \text{etc.}\\ \text{with } m = 2,\ldots,q;\quad & N^{(E)} = 12(q-1);\quad q \geq 2\end{aligned} \tag{14.1.39}$$

$$\begin{aligned}\text{Face mode:}\quad & \Phi_{mn}^{(F1)} = \tfrac{1}{2}(1-\eta)G_m(\xi)G_n(\eta)\\ & \Phi_{mn}^{(F2)} = \tfrac{1}{2}(1+\xi)G_m(\eta)G_n(\zeta)\\ & \text{etc.}\\ \text{with } m,n = 2,\ldots,q-2;\quad & (m+n) = 4,\ldots,q;\\ & N^{(F)} = 3(q-2)(q-3);\quad q \geq 4\end{aligned} \tag{14.1.40}$$

$$\text{Interior mode:} \quad \Phi^{(I)}_{mnp} = G_m(\xi)G_n(\eta)G_p(\zeta) \tag{14.1.41}$$

$$\text{with } m, n, p = 2, \ldots, q-4; \quad (m+n+p) = 6, \ldots, q;$$
$$N^{(I)} = (q-3)(q-4)(q-5)/6; \quad q \geq 6$$

In addition to the above polynomials ($S1$), we may use an optional space ($S2$) in which $(q-1)^2$ face modes and $(q-1)^3$ interior modes ($q \geq 2$) are applied.

14.1.3 TWO-DIMENSIONAL PROBLEMS

Spectral element methods may be implemented through the generalized Galerkin scheme. A more rigorous approach such as the FDV-FEM technique introduced in Chapter 13 can be combined with the spectral functions. This is particularly useful for dealing with high-speed flows where shock wave/turbulent boundary layer interactions occur.

In general, the spectral element formulation begins with the Galerkin integral expressed in the following form:

For Corner Nodes

$$\int_\Omega \Phi_\alpha \mathbf{R}(\Delta\mathbf{U}) d\Omega = 0 \tag{14.1.42a}$$

For Side Modes

$$\int_\Omega \Phi^{(S)}_m \mathbf{R}(\Delta\mathbf{U}) d\Omega = 0 \tag{14.1.42b}$$

For Interior Modes

$$\int_\Omega \Phi^{(I)}_{mn} \mathbf{R}(\Delta\mathbf{U}) d\Omega = 0 \tag{14.1.42c}$$

where the conservation variables $\mathbf{U}$ in the residual $\mathbf{R}(\Delta\mathbf{U})$ of the Navier-Stokes system of equations are approximated by the trial functions, and the source terms are assumed to be zero.

Substituting (14.1.33) into (14.1.42) yields the matrix equations,

$$\begin{bmatrix} A_{\alpha\beta}\delta_{rs} + B_{\alpha\beta rs} & A^{\delta}_{\alpha n}\delta_{rs} + B^{\delta}_{\alpha nrs} & A_{\alpha np}\delta_{rs} + B_{\alpha nprs} \\ A^{\gamma}_{m\beta}\delta_{rs} + B^{\gamma}_{m\beta rs} & A^{\gamma\delta}_{mn}\delta_{rs} + C^{\gamma\delta}_{mnrs} & A^{\gamma}_{mnp}\delta_{rs} + C^{\gamma}_{mnprs} \\ A_{mk\beta}\delta_{rs} + B_{mk\beta rs} & A^{\delta}_{mkn}\delta_{rs} + C^{\delta}_{mknrs} & A_{mknp}\,\delta_{rs} + D_{mknprs} \end{bmatrix} \begin{bmatrix} \Delta U_{\beta s} \\ \Delta \hat{U}^{\delta}_{ns} \\ \Delta \hat{U}_{nps} \end{bmatrix}^{n+1}$$
$$= \begin{bmatrix} W_{\alpha r} \\ \hat{W}^{\gamma}_{mr} \\ \hat{W}_{mkr} \end{bmatrix}^{n} \tag{14.1.43}$$

where α, β denote the product of the global corner node number times the total number of physical variables, whereas m, n, p, and q refer to degrees of freedom from the side and internal modes of Legendre polynomials with $\gamma, \delta = 1, 4$ and r, s denoting the number of conservation variables (4 in two dimensions and 5 in three dimensions).

If the residual $\mathbf{R}(\Delta\mathbf{U})$ is chosen to be the same as (13.1.2) for the FDV-FEM scheme without source terms, we obtain the matrix entries of (14.1.43) as follows:

$$
\begin{aligned}
A_{\alpha\beta} &= \int_\Omega \Phi_\alpha \Phi_\beta \, d\Omega \qquad A^{\delta}_{\alpha n} = \int_\Omega \Phi_\alpha \hat{\Phi}^{\delta}_{n} \, d\Omega \qquad A_{\alpha np} = \int_\Omega \Phi_\alpha \hat{\Phi}_{np} \, d\Omega \\
A^{\gamma}_{m\beta} &= \int_\Omega \hat{\Phi}^{\gamma}_{m} \Phi_\beta \, d\Omega \qquad A^{\gamma\delta}_{mn} = \int_\Omega \hat{\Phi}^{\gamma}_{m} \hat{\Phi}^{\delta}_{n} \, d\Omega \qquad A^{\gamma}_{mnp} = \int_\Omega \hat{\Phi}^{\gamma}_{m} \hat{\Phi}_{np} \, d\Omega \\
A_{mk\beta} &= \int_\Omega \hat{\Phi}_{mk} \Phi_\beta \, d\Omega \quad A^{\delta}_{mkn} = \int_\Omega \hat{\Phi}_{mk} \hat{\Phi}^{\delta}_{n} \, d\Omega \quad A_{mknp} = \int_\Omega \hat{\Phi}_{mk} \hat{\Phi}_{np} \, d\Omega
\end{aligned}
\tag{14.1.44}
$$

$$
\begin{aligned}
B_{\alpha\beta rs} &= \int_\Omega \Big\{ \Delta t \left[-s_1 a_{irs} \Phi_{\alpha,i} \Phi_\beta - s_3 (b_{irs} \Phi_{\alpha,i} \Phi_\beta + c_{ijrs} \Phi_{\alpha,i} \Phi_{\beta,j}) \right] \\
&\quad + \frac{\Delta t^2}{2} ([s_2 (a_{irt} a_{jts} + b_{irt} a_{jts}) \Phi_{\alpha,i} \Phi_{\beta,j} - d_{rt} a_{its} \Phi_{\alpha,i} \Phi_\beta] \\
&\quad + s_4 [(a_{irt} b_{jts} + b_{irt} b_{jts} - d_{rt} c_{ijts}) \Phi_{\alpha,i} \Phi_{\beta,j} - d_{rt} b_{its} \Phi_{\alpha,i} \Phi_\beta]) \Big\} \, d\Omega \\
B^{\delta}_{\alpha nrs} &= \int_\Omega \Big\{ -\Delta t \left[(s_1 a_{irs} + s_3 b_{irs}) \Phi_{\alpha,i} \hat{\Phi}^{\delta}_{n} + s_3 c_{ijrs} \Phi_{\alpha,i} \hat{\Phi}_{n,j} \right] \\
&\quad + \frac{\Delta t^2}{2} (s_2 d_{ijrs} + s_4 e_{ijrs}) \Phi_{\alpha,i} \hat{\Phi}^{\delta}_{n,j} \Big\} d\Omega
\end{aligned}
$$

with

$$
\begin{aligned}
d_{ijrs} &= a_{irt} a_{jts} + b_{irt} a_{jts} \\
e_{ijrs} &= a_{irt} b_{jts} + b_{irt} b_{jts} \\
B_{\alpha nprs} &= \int_\Omega \Big\{ -\Delta t \left[(s_1 a_{irs} + s_3 b_{irs}) \Phi_{\alpha,i} \hat{\Phi}_{np} + s_3 c_{ijrs} \Phi_{\alpha,i} \hat{\Phi}_{np,j} \right] \\
&\quad + \frac{\Delta t^2}{2} (s_2 d_{ijrs} + s_4 e_{ijrs}) \Phi_{\alpha,i} \hat{\Phi}_{np,j} \Big\} d\Omega \\
B^{\gamma}_{m\beta rs} &= \int_\Omega \Big\{ -\Delta t \left[(s_1 a_{irs} + s_3 b_{irs}) \hat{\Phi}^{\gamma}_{m,i} \Phi_\beta + s_3 c_{ijrs} \hat{\Phi}^{\gamma}_{m,i} \Phi_{\beta,j} \right] \\
&\quad + \frac{\Delta t^2}{2} (s_2 d_{ijrs} + s_4 e_{ijrs}) \hat{\Phi}^{\gamma}_{m,i} \Phi_{\beta,j} \Big\} d\Omega \\
C^{\gamma\delta}_{mnrs} &= \int_\Omega \Big\{ -\Delta t \left[(s_1 a_{irs} + s_3 b_{irs}) \hat{\Phi}^{\gamma}_{m,i} \hat{\Phi}^{\delta}_{n} + s_3 c_{ijrs} \hat{\Phi}^{\gamma}_{m,i} \hat{\Phi}^{\delta}_{n,j} \right] \\
&\quad + \frac{\Delta t^2}{2} (s_2 d_{ijrs} + s_4 e_{ijrs}) \hat{\Phi}^{\gamma}_{m,i} \hat{\Phi}^{\delta}_{n,j} \Big\} d\Omega \\
C^{\gamma}_{mnprs} &= \int_\Omega \Big\{ -\Delta t \left[(s_1 a_{irs} + s_3 b_{irs}) \hat{\Phi}^{\gamma}_{m,i} \hat{\Phi}_{np} + s_3 c_{ijrs} \hat{\Phi}^{\gamma}_{m,i} \hat{\Phi}_{np,j} \right] \\
&\quad + \frac{\Delta t^2}{2} (s_2 d_{ijrs} + s_4 e_{ijrs}) \hat{\Phi}^{\gamma}_{m,i} \hat{\Phi}_{np,j} \Big\} d\Omega
\end{aligned}
$$

$$
\begin{aligned}
B_{mk\beta rs} &= \int_{\Omega} \Big\{ -\Delta t \left[(s_1 a_{irs} + s_3 b_{irs}) \hat{\Phi}_{mk,i} \Phi_{\beta} + s_3 c_{ijrs} \hat{\Phi}_{mk,i} \Phi_{\beta,j} \right] \\
&\quad + \frac{\Delta t^2}{2} (s_2 d_{ijrs} + s_4 e_{ijrs}) \hat{\Phi}_{mk,i} \Phi_{\beta,j} \Big\} d\Omega \\
C^{\delta}_{mknrs} &= \int_{\Omega} \Big\{ -\Delta t \left[(s_1 a_{irs} + s_3 b_{irs}) \hat{\Phi}_{mk,i} \hat{\Phi}^{\delta}_{n} + s_3 c_{ijrs} \hat{\Phi}_{mk,i} \hat{\Phi}^{\delta}_{n,j} \right] \\
&\quad + \frac{\Delta t^2}{2} (s_2 d_{ijrs} + s_4 e_{ijrs}) \hat{\Phi}_{mk,i} \hat{\Phi}^{\delta}_{n,j} \Big\} d\Omega \\
D_{mknprs} &= \int_{\Omega} \Big\{ -\Delta t \left[(s_1 a_{irs} + s_3 b_{irs}) \hat{\Phi}_{mk,i} \hat{\Phi}_{np} + s_3 c_{ijrs} \hat{\Phi}_{mk,i} \hat{\Phi}_{np,j} \right] \\
&\quad + \frac{\Delta t^2}{2} (s_2 d_{ijrs} + s_4 e_{ijrs}) \hat{\Phi}_{mk,i} \hat{\Phi}_{np,j} \Big\} d\Omega
\end{aligned} \tag{14.1.45}
$$

$$
W_{\alpha r} = H^n_{\alpha r} + N^n_{\alpha r} + \overline{N}^{n+1}_{\alpha r} \tag{14.1.46}
$$

with

$$
\begin{aligned}
H^n_{\alpha r} &= \int_{\Omega} \Big\{ \Delta t \, \Phi_{\alpha,i} \Phi_{\beta} \left(F^n_{\beta ir} + G^n_{\beta ir} \right) - \frac{\Delta t^2}{2} (a_{irs} + b_{irs}) \Phi_{\alpha,i} \Phi_{\beta,j} \left(F^n_{\beta js} + G^n_{\beta js} \right) \Big\} d\Omega \\
N^n_{\alpha r} &= \int_{\Gamma} \overset{*}{\Phi}_{\alpha} \Big[-\Delta t \left(F^n_{ir} + G^n_{ir} \right) + \frac{\Delta t^2}{2} (a_{irs} + b_{irs}) \left(F^n_{js,j} + G^n_{js,j} \right) \Big] n_i d\Gamma \\
\overline{N}^{n+1}_{\alpha r} &= \int_{\Gamma} \overset{*}{\Phi}_{\alpha} \Big\{ -\Delta t \left[(s_1 a_{irs} + s_3 b_{irs}) \Delta U^{n+1}_{s} + s_3 \, c_{ijrs} \Delta U^{n+1}_{s,j} \right] \\
&\quad + \frac{\Delta t^2}{2} (s_2 d_{ijrs} + s_4 e_{ijrs}) \Delta U^{n+1}_{s,j} \Big\} n_i \, d\Gamma \\
\hat{W}^{\gamma}_{mr} &= \int_{\Omega} \Big\{ \Delta t \, \hat{\Phi}^{\gamma}_{m,i} \Phi_{\beta} \left(F^n_{\beta ir} + G^n_{\beta ir} \right) - \frac{\Delta t^2}{2} (a_{irs} + b_{irs}) \hat{\Phi}^{\gamma}_{m,i} \Phi_{\beta,j} \left(F^n_{\beta js} + G^n_{\beta js} \right) \Big\} d\Omega \\
&\quad + \int_{\Gamma} \overset{*}{\hat{\Phi}}^{\gamma}_{m} \Big\{ \Delta t \left[-s_1 \left(a_{irs} \Delta U^{n+1}_{s} \right) - s_3 \left(b_{irs} \Delta U^{n+1}_{s} + c_{ijrs} \Delta U^{n+1}_{s,j} \right) \right] \\
&\quad + \frac{\Delta t^2}{2} \left[s_2 \left(a_{irt} a_{jts} + b_{irt} a_{jts} \right) \Delta U^{n+1}_{s,j} + s_4 \left(a_{irt} b_{jts} + b_{irt} b_{jts} \right) \Delta U^{n+1}_{s,j} \right] \Big\} n_i \, d\Gamma \\
&\quad + \int_{\Gamma} \overset{*}{\hat{\Phi}}^{\gamma}_{m} \Big\{ -\Delta t \left(F^n_{ir} + G^n_{ir} \right) + \frac{\Delta t^2}{2} (a_{irs} + b_{irs}) \left(F^n_{js,j} + G^n_{js,j} - B^n_{s} \right) \Big\} n_i \, d\Gamma \\
\hat{W}_{mkr} &= \int_{\Omega} \Big\{ \Delta t \, \hat{\Phi}_{mk,i} \Phi_{\beta} \left(F^n_{\beta ir} + G^n_{\beta ir} \right) \\
&\quad - \frac{\Delta t^2}{2} (a_{irs} + b_{irs}) \hat{\Phi}_{mk,i} \Phi_{\beta,j} \left(F^n_{\beta js} + G^n_{\beta js} \right) \Big\} d\Omega
\end{aligned} \tag{14.1.47}
$$

If the Neumann boundary conditions for spectral modes are not specified, then, by definition, $\hat{\Phi}^*_m = \hat{\Phi}^*_{mn} = 0$ and only the corner nodes are subjected to the Neumann boundary conditions. However, these spectral Neumann boundary conditions may be computed and added after the initial corner node computation, resulting in possible improvements for the final solution.

The orthogonal properties of the Legendre polynomials give rise to sparse local matrices. For example, the following orthogonal properties arise for diffusion terms:

$\int_\Omega \Phi_{N,i}\hat{\Phi}^{\delta}_{n,i}\, d\Omega \neq 0$ if and only if $n = 2$, or 3, zero otherwise

$\int_\Omega \Phi_{N,i}\hat{\Phi}_{np,i}\, d\Omega \equiv 0$ always

$\int_\Omega \hat{\Phi}^{\gamma}_{m,i}\Phi^{\delta}_{n,i}\, d\Omega \neq 0$ if and only if $\gamma - \delta =$ even and $m = n$ or $m = n \pm 2$, zero otherwise

$\int_\Omega \hat{\Phi}^{\delta}_{m,i}\hat{\Phi}_{np,i}\, d\Omega \neq 0$ if and only if $m = p$ and $n = 2$ or 3, with $\gamma = 1$ or 3; $m = n$ and $p = 2$ or 3, with $\gamma = 2$ or 4; zero otherwise

$\int_\Omega \hat{\Phi}_{mk,i}\,\hat{\Phi}_{np,i}\, d\Omega \neq 0$ if and only if $m = n$ or $m = n \pm 2$ and $k = p$; $k = p$ or $k = p \pm 2$, and $m = n$; zero otherwise

It should be noted that these results are also obtained by using the Gaussian quadrature routine for integration.

Although the direct solution of (14.1.43) can be obtained, a number of other options are available. For example, we may initially consider only the corner node equations,

$$(A_{\alpha\beta}\delta_{rs} + B_{\alpha\beta rs})\,\Delta U^{n+1}_{\beta s} = W_{\alpha r} \tag{14.1.48}$$

The solution of (14.1.48) can be subsequently applied to the side-mode and edge-mode equations of (14.1.43) to solve

$$\begin{bmatrix} A^{\gamma\delta}_{mn}\delta_{rs} + C^{\gamma\delta}_{mnrs} & A^{\gamma}_{mnp}\delta_{rs} + C^{\gamma}_{mnprs} \\ A^{\delta}_{mkn}\delta_{rs} + C^{\delta}_{mknrs} & A_{mknp}\,\delta_{rs} + D_{mknprs} \end{bmatrix} \begin{bmatrix} \Delta\hat{U}^{\delta}_{ns} \\ \Delta\hat{U}_{nps} \end{bmatrix} = \begin{bmatrix} \hat{W}^{\gamma}_{mr} - X^{\gamma}_{mr} \\ \hat{W}_{mkr} - X_{mkr} \end{bmatrix} \tag{14.1.49}$$

where

$$X^{\gamma}_{mr} = \left(A^{\gamma}_{m\beta}\delta_{rs} + B^{\gamma}_{m\beta rs}\right)\Delta U_{\beta s}$$

$$X_{mkr} = \left(A_{mk\beta}\delta_{rs} + B_{mk\beta rs}\right)\Delta U_{\beta s}$$

This allows (14.1.48) to be revised as

$$(A_{\alpha\beta}\delta_{rs} + B_{\alpha\beta rs})\Delta U^{n+1}_{\beta s} = W_{\alpha r} - \left(A^{\delta}_{\alpha n}\delta_{rs} + B^{\delta}_{\alpha nrs}\right)\Delta\hat{U}^{\delta}_{ns} - (A_{\alpha np}\delta_{rs} + B_{\alpha nprs})\Delta\hat{U}_{nps} \tag{14.1.50}$$

This approach resembles the so-called static condensation performed in reverse order. Thus, the solutions between (14.1.50) and (14.1.49) may be repeated until the desired convergence is obtained.

Notice that one advantage of this formulation is that, although the corner node isoparametric finite element function remains linear, the side and interior mode spectral orders can vary from element to element (Figure 14.1.2) as high as desired in order to simulate particular physical phenomena such as turbulence. Furthermore, the corner node linear isoparametric functions allow the computation of variables only at the

corner nodes, irrespective of high order spectral functions chosen for side and interior modes.

Remark: It has been demonstrated that the SEM is effective for nonlinear problems, particularly for problems with singularities such as in shock waves and with high gradients such as in turbulence. For linear partial differential equations with smooth exact solutions, the numerical analysis by SEM may produce results which are worse than those of linear FEM (corner nodes only). This is an important observation in that the imposition of the higher order functions (Legendre polynomials) upon the linear solution surface may distort the numerical solution. This distortion may be drastic in some cases. Therefore, SEM is not recommended for linear problems. To illustrate, consider the results shown in the example below of the SEM solutions of a Laplace equation in comparison with the FEM solutions.

14.1.4 THREE-DIMENSIONAL PROBLEMS

For three-dimensional problems, the Galerkin integral is expressed in the following form:

For Corner Nodes

$$\int_{\Omega} \Phi_{\alpha} \mathbf{R}(\Delta \mathbf{U}) d\Omega = 0 \tag{14.1.51a}$$

For Edge Modes

$$\int_{\Omega} \Phi_{m}^{(E)} \mathbf{R}(\Delta \mathbf{U}) d\Omega = 0 \tag{14.1.51b}$$

For Face Nodes

$$\int_{\Omega} \Phi_{mn}^{(F)} \mathbf{R}(\Delta \mathbf{U}) d\Omega = 0 \tag{14.1.51c}$$

For Interior Nodes

$$\int_{\Omega} \Phi_{mnp}^{(I)} \mathbf{R}(\Delta \mathbf{U}) d\Omega = 0 \tag{14.1.51d}$$

Substituting (14.1.16) into (14.1.1) gives

$$\begin{bmatrix} A_{\alpha\beta}\delta_{rs} + B_{\alpha\beta rs} & A^{\delta}_{\alpha n}\delta_{rs} + B^{\delta}_{\alpha nrs} & A^{\eta}_{\alpha np}\delta_{rs} + B^{\eta}_{\alpha nprs} & A_{\alpha npq}\delta_{rs} + B_{\alpha npqrs} \\ A^{\gamma}_{m\beta}\delta_{rs} + B^{\gamma}_{m\beta rs} & A^{\gamma\delta}_{mn}\delta_{rs} + C^{\gamma\delta}_{mnrs} & A^{\gamma\eta}_{mnp}\delta_{rs} + C^{\gamma\eta}_{mnprs} & A^{\gamma}_{mnpq}\delta_{rs} + C^{\gamma}_{mnpqrs} \\ A^{\xi}_{mk\beta}\delta_{rs} + B^{\xi}_{mk\beta rs} & A^{\xi\delta}_{mkn}\delta_{rs} + C^{\xi\delta}_{mknrs} & A^{\xi\eta}_{mknp}\delta_{rs} + D^{\xi\eta}_{mknprs} & A^{\xi}_{mknpq}\delta_{rs} + D^{\xi}_{mknpqrs} \\ A_{mku\beta}\delta_{rs} + B_{mku\beta rs} & A^{\delta}_{mkun}\delta_{rs} + C^{\delta}_{mkunrs} & A^{\eta}_{mkunp}\delta_{rs} + D^{\eta}_{mkunprs} & A_{mkunpq}\delta_{rs} + E_{mkunpqrs} \end{bmatrix}$$

$$\times \begin{bmatrix} \Delta U_{\beta s} \\ \Delta \hat{U}^{\delta}_{ns} \\ \Delta \hat{U}^{\eta}_{nps} \\ \Delta \hat{U}_{npqs} \end{bmatrix}^{n+1} = \begin{bmatrix} W_{\alpha r} \\ \hat{W}^{\gamma}_{mr} \\ \hat{W}^{\xi}_{mkr} \\ \hat{W}_{mkur} \end{bmatrix}^{n} \tag{14.1.52}$$

with $\gamma, \delta = 1 \to 12; \xi, \eta = 1 \to 8$; $m, k, n, p, q,$ = degrees of freedom from edge, face, and interior modes; α, β = corner node variables; r, s = conservation variable degrees of freedom.

Note that all matrix entries are identical to the two-dimensional case with the following exception:

$$A_{\alpha npq} = \int_\Omega \Phi_\alpha \hat{\Phi}_{npq}\, d\Omega \quad A_{mku\beta} = \int_\Omega \hat{\Phi}_{mku} \Phi_\beta\, d\Omega \quad A^{\gamma}_{mnpq} = \int_\Omega \hat{\Phi}^{\gamma}_{m} \hat{\Phi}_{npq}\, d\Omega$$

$$A^{\delta}_{mkun} = \int_\Omega \hat{\Phi}_{mku} \hat{\Phi}^{\delta}_{n}\, d\Omega \quad A^{\xi}_{mknpq} = \int_\Omega \hat{\Phi}^{\xi}_{mk} \hat{\Phi}_{npq}\, d\Omega \quad A^{\eta}_{mkunp} = \int_\Omega \hat{\Phi}_{mku} \hat{\Phi}^{\eta}_{np}\, d\Omega$$

$$A_{mkunpq} = \int_\Omega \hat{\Phi}_{mku} \hat{\Phi}_{npq}\, d\Omega \tag{14.1.53}$$

$$B_{\alpha npqrs} = \int_\Omega \left\{ -\Delta t[(s_1 a_{irs} + s_3 b_{irs})\Phi_{\alpha,i} \hat{\Phi}_{npq} + s_3 c_{ijrs} \Phi_{\alpha,i} \hat{\Phi}_{npq,j}] + \frac{\Delta t^2}{2}(s_2 d_{ijrs} + s_4 e_{ijrs})\Phi_{\alpha,i} \hat{\Phi}_{npq,j} \right\} d\Omega$$

$$B_{mku\beta rs} = \int_\Omega \left\{ -\Delta t\,[(s_1 a_{irs} + s_3 b_{irs})\hat{\Phi}_{mku,i} \Phi_\beta + s_3 c_{ijrs} \hat{\Phi}_{mku,i} \Phi_{\beta,j}] + \frac{\Delta t^2}{2}(s_2 d_{ijrs} + s_4 e_{ijrs})\hat{\Phi}_{mku,i} \Phi_{\beta,j} \right\} d\Omega$$

$$C^{\delta}_{mkunrs} = \int_\Omega \left\{ -\Delta t\,[(s_1 a_{irs} + s_3 b_{irs})\hat{\Phi}_{mku,i} \hat{\Phi}^{\delta}_{n} + s_3 c_{ijrs} \hat{\Phi}_{mku,i} \hat{\Phi}^{\delta}_{n,j}] + \frac{\Delta t^2}{2}(s_2 d_{ijrs} + s_4 e_{ijrs})\hat{\Phi}_{mku,i} \hat{\Phi}^{\delta}_{n,j} \right\} d\Omega$$

$$C^{\gamma}_{mnpqrs} = \int_\Omega \left\{ -\Delta t\,[(s_1 a_{irs} + s_3 b_{irs})\hat{\Phi}^{\gamma}_{m,i} \hat{\Phi}_{npq} + s_3 c_{ijrs} \hat{\Phi}^{\gamma}_{m,i} \hat{\Phi}_{npq,j}] + \frac{\Delta t^2}{2}(s_2 d_{ijrs} + s_4 e_{ijrs})\hat{\Phi}^{\gamma}_{m,i} \hat{\Phi}_{npq,j} \right\} d\Omega$$

$$D^{\xi}_{mknpqrs} = \int_\Omega \left\{ -\Delta t\,[(s_1 a_{irs} + s_3 b_{irs})\hat{\Phi}^{\xi}_{mk,i} \hat{\Phi}_{npq} + s_3 c_{ijrs} \hat{\Phi}^{\xi}_{mk,i} \hat{\Phi}_{npq,j}] + \frac{\Delta t^2}{2}(s_2 d_{ijrs} + s_4 e_{ijrs})\hat{\Phi}^{\xi}_{mk,i} \hat{\Phi}_{npq,j} \right\} d\Omega$$

$$D^{\eta}_{mkunprs} = \int_\Omega \left\{ -\Delta t\,[(s_1 a_{irs} + s_3 b_{irs})\hat{\Phi}_{mku,i} \hat{\Phi}^{\eta}_{np} + s_3 c_{ijrs} \hat{\Phi}_{mku,i} \hat{\Phi}^{\eta}_{np,j}] + \frac{\Delta t^2}{2}(s_2 d_{ijrs} + s_4 e_{ijrs})\hat{\Phi}_{mku,i} \hat{\Phi}^{\eta}_{np,j} \right\} d\Omega$$

$$E_{mkunpqrs} = \int_\Omega \left\{ -\Delta t\,[(s_1 a_{irs} + s_3 b_{irs})\hat{\Phi}_{mku,i} \hat{\Phi}_{npq} + s_3 c_{ijrs} \hat{\Phi}_{mku,i} \hat{\Phi}_{npq,j}] + \frac{\Delta t^2}{2}(s_2 d_{ijrs} + s_4 e_{ijrs})\hat{\Phi}_{mku,i} \hat{\Phi}_{npq,j} \right\} d\Omega \tag{14.1.54}$$

$$\hat{W}^{\gamma}_{mr} = \int_{\Omega} \left\{ \Delta t\, \hat{\Phi}^{\gamma}_{m,i} \Phi_{\beta} \left(F^{n}_{\beta ir} + G^{n}_{\beta ir} \right) - \frac{\Delta t^2}{2} (a_{irs} + b_{irs}) \hat{\Phi}^{\gamma}_{m,i} \Phi_{\beta,j} \left(F^{n}_{\beta js} + G^{n}_{\beta js} \right) \right\} d\Omega$$
$$+ \int_{\Gamma} \overset{*}{\hat{\Phi}}{}^{\gamma}_{m} \left\{ \Delta t \left[-s_1 \left(a_{irs} \Delta U^{n+1}_{s} \right) - s_3 \left(b_{irs} \Delta U^{n+1}_{s} + c_{ijrs} \Delta U^{n+1}_{s,j} \right) \right] \right.$$
$$\left. + \frac{\Delta t^2}{2} \left[s_2 (a_{irt} a_{jts} + b_{irt} a_{jts}) \Delta U^{n+1}_{s,j} + s_4 (a_{irt} b_{jts} + b_{irt} b_{jts}) \Delta U^{n+1}_{s,j} \right] \right\} n_i \, d\Gamma$$
$$+ \int_{\Gamma} \overset{*}{\hat{\Phi}}{}^{\gamma}_{m} \left\{ -\Delta t \left(F^{n}_{ir} + G^{n}_{ir} \right) + \frac{\Delta t^2}{2} (a_{irs} + b_{irs}) \left(F^{n}_{js,j} + G^{n}_{js,j} - B^{n}_{s} \right) \right\} n_i \, d\Gamma$$

$$\hat{W}^{\xi}_{mkr} = \int_{\Omega} \left\{ \Delta t\, \hat{\Phi}^{\xi}_{mk,i} \Phi_{\beta} \left(F^{n}_{\beta ir} + G^{n}_{\beta ir} \right) - \frac{\Delta t^2}{2} (a_{irs} + b_{irs}) \hat{\Phi}^{\xi}_{mk,i} \Phi_{\beta,j} \left(F^{n}_{\beta js} + G^{n}_{\beta js} \right) \right\} d\Omega$$
$$+ \int_{\Gamma} \overset{*}{\hat{\Phi}}{}^{\gamma}_{mk} \left\{ \Delta t \left[-s_1 \left(a_{irs} \Delta U^{n+1}_{s} \right) - s_3 \left(b_{irs} \Delta U^{n+1}_{s} + c_{ijrs} \Delta U^{n+1}_{s,j} \right) \right] \right.$$
$$\left. + \frac{\Delta t^2}{2} \left[s_2 (a_{irt} a_{jts} + b_{irt} a_{jts}) \Delta U^{n+1}_{s,j} + s_4 (a_{irt} b_{jts} + b_{irt} b_{jts}) \Delta U^{n+1}_{s,j} \right] \right\} n_i \, d\Gamma$$
$$+ \int_{\Gamma} \overset{*}{\hat{\Phi}}{}^{\gamma}_{mk} \left\{ -\Delta t \left(F^{n}_{ir} + G^{n}_{ir} \right) + \frac{\Delta t^2}{2} (a_{irs} + b_{irs}) \left(F^{n}_{js,j} + G^{n}_{js,j} - B^{n}_{s} \right) \right\} n_i \, d\Gamma$$

$$\hat{W}_{mkur} = \int_{\Omega} \left\{ \Delta t\, \hat{\Phi}_{mku,i} \Phi_{\beta} \left(F^{n}_{\beta ir} + G^{n}_{\beta ir} \right) \right.$$
$$\left. - \frac{\Delta t^2}{2} (a_{irs} + b_{irs}) \hat{\Phi}_{mku,i} \Phi_{\beta,j} \left(F^{n}_{\beta js} + G^{n}_{\beta js} \right) \right\} d\Omega \tag{14.1.55}$$

As mentioned earlier for the case of two dimensions, the Neumann boundary conditions involved in all spectral degrees of freedom do not exist and are not applied, initially. However, they may be computed and added after the initial corner node computation. As in 2-D, we begin with

$$(A_{\alpha\beta} \delta_{rs} + B_{\alpha\beta rs}) \Delta U^{n+1}_{\beta s} = W^{n}_{\alpha r} \tag{14.1.56}$$

In this process, the FDV-FEM computations are carried out with h-adaptivity until all shock waves are resolved. The next step is to resolve turbulent microscales using the spectral portion of the computations

$$\begin{bmatrix} A^{\gamma\delta}_{mn} \delta_{rs} + C^{\gamma\delta}_{mnrs} & A^{\gamma\eta}_{mnp} \delta_{rs} + C^{\gamma\eta}_{mnprs} & A^{\gamma}_{mnpq} \delta_{rs} + C^{\gamma}_{mnpqrs} \\ A^{\xi\delta}_{mkn} \delta_{rs} + C^{\xi\delta}_{mknrs} & A^{\xi\eta}_{mknp} \delta_{rs} + D^{\xi\eta}_{mknprs} & A^{\xi}_{mknpq} \delta_{rs} + D^{\xi}_{mknpqrs} \\ A^{\delta}_{mkun} \delta_{rs} + C^{\delta}_{mkunrs} & A^{\eta}_{mkunp} \delta_{rs} + D^{\eta}_{mkunprs} & A_{mkunpq} \delta_{rs} + E_{mkunpqrs} \end{bmatrix} \begin{bmatrix} \Delta \hat{U}^{\delta}_{ns} \\ \Delta \hat{U}^{\eta}_{nps} \\ \Delta \hat{U}_{npqs} \end{bmatrix}$$
$$= \begin{bmatrix} \hat{W}^{\gamma}_{mr} \\ \hat{W}^{\xi}_{mkr} \\ \hat{W}_{mkur} \end{bmatrix} - \begin{bmatrix} X^{\gamma}_{mr} \\ X^{\xi}_{mkr} \\ X_{mkur} \end{bmatrix} \tag{14.1.57}$$

where

$$X^{\gamma}_{mr} = \left(A^{\gamma}_{m\beta} \delta_{rs} + B^{\gamma}_{m\beta rs} \right) \Delta U_{\beta s}$$
$$X^{\xi}_{mkr} = \left(A^{\xi}_{mk\beta} \delta_{rs} + B^{\xi}_{mk\beta rs} \right) \Delta U_{\beta s}$$
$$X_{npqs} = \left(A_{mkuu\beta} \delta_{rs} + B_{mku\beta rs} \right) \Delta U_{\beta s}$$

which act as source terms or coupling effect of the corner nodes upon spectral behavior through side, face, and interior modes. The final step is to combine (14.1.56) and (14.1.57) by

$$(A_{\alpha\beta}\delta_{rs} + B_{\alpha\beta rs})\,\Delta U_{\beta s}^{n+1} = W_{\alpha r}^{n} + Y_{\alpha r} \tag{14.1.58}$$

with

$$\begin{aligned} Y_{\alpha r} \;=\; & \left(A_{\alpha n}^{\delta}\delta_{rs} + B_{\alpha\beta rs}^{\delta}\right)\Delta\hat{U}_{ns}^{\delta} + \left(A_{\alpha np}^{\eta}\delta_{rs} + B_{\alpha nprs}^{\eta}\right)\Delta\hat{U}_{nps}^{\eta} \\ & + (A_{\alpha npq}\delta_{rs} + B_{\alpha npqrs})\Delta\hat{U}_{npqs} \end{aligned}$$

Thus, the convergence toward shock wave turbulent boundary layer interactions can be achieved through iterations between (14.1.57) and (14.1.58). Note that in this process, the convection implicitness parameters s_1 and s_2 are held constant, whereas the diffusion implicitness parameters s_3 and s_4 are updated through Reynolds numbers. Some examples are shown in Section 14.4.

14.2 LEAST SQUARES METHODS

The least squares methods (LSM) have been used in FEM by a number of authors such as Lynn [1974], Bramble and Shatz [1970], Fix and Gunzburger [1978], Carey and Jiang [1987], among others. In LSM, the inner products of the governing equations are constructed, which are then differentiated (minimized) with respect to the nodal values of the variables. The integration by parts which is normally required in the standard Galerkin method is not involved. As a consequence, higher order derivatives remain, which will then require higher order trial functions. The basic formulation strategies are described next.

14.2.1 LSM FORMULATION FOR THE NAVIER-STOKES SYSTEM OF EQUATIONS

To illustrate the procedure, let us consider the Navier-Stokes system of equations,

$$\mathbf{R} = \frac{\partial \mathbf{U}}{\partial t} + \mathbf{a}_i \frac{\partial \mathbf{U}}{\partial x_i} + \mathbf{b}_i \frac{\partial \mathbf{U}}{\partial x_i} + \mathbf{c}_{ij} \frac{\partial^2 \mathbf{U}}{\partial x_i \partial x_j} - \mathbf{B} \tag{14.2.1}$$

where

$$\mathbf{U} = \Phi_\alpha \mathbf{U}_\alpha \tag{14.2.2}$$

The least squares formulation of (14.2.1) leads to

$$\frac{\partial}{\partial \mathbf{U}_\alpha}\frac{1}{2}(\mathbf{R},\mathbf{R}) = \frac{\partial}{\partial \mathbf{U}_\alpha}\int_\Omega \frac{1}{2}\mathbf{R}^2 d\Omega = 0$$

This leads to

$$\int_\Omega W_\alpha \mathbf{R}\, d\Omega = 0 \tag{14.2.3}$$

with the test function W_α given by

$$W_\alpha = \frac{\partial \mathbf{R}}{\partial \mathbf{U}_\alpha} \tag{14.2.4}$$

or

$$W_\alpha = \frac{\partial \Phi_\alpha}{\partial t} + \mathbf{a}_i \frac{\partial \Phi_\alpha}{\partial x_i} + \mathbf{b}_i \frac{\partial \Phi_\alpha}{\partial x_i} + \mathbf{c}_{ij} \frac{\partial^2 \Phi_\alpha}{\partial x_i \partial x_j} \tag{14.2.5}$$

It is seen that the trial function Φ_α is not a function of time and the first term in (14.2.5) must vanish. To avoid this situation, we rewrite (14.2.1) in the form

$$\mathbf{R} = \mathbf{U}^{n+1} - \mathbf{U}^n + \Delta t \left(\mathbf{a}_i \frac{\partial \mathbf{U}}{\partial x_i} + \mathbf{b}_i \frac{\partial \mathbf{U}}{\partial x_i} + \mathbf{c}_{ij} \frac{\partial^2 \mathbf{U}}{\partial x_i \partial x_j} - \mathbf{B} \right) \tag{14.2.6}$$

This will allow the test function W_α to be written as

$$W_\alpha = \frac{\partial \mathbf{R}}{\partial \mathbf{U}_\alpha^{n+1}} = \Phi_\alpha + \frac{\Delta t}{2} \left(\mathbf{a}_i \Phi_{\alpha,i} + \mathbf{b}_i \Phi_{\alpha,i} + \mathbf{c}_{ij} \Phi_{\alpha,ij} \right) \tag{14.2.7}$$

with $U = (U^{n+1} + U^n)/2$. Thus, (14.2.3) takes the form

$$K_{\alpha\beta} \mathbf{U}_\beta^{n+1} = \mathbf{F}_\alpha^n \tag{14.2.8}$$

where the stiffness matrix $K_{\alpha\beta}$ is of the form

$$\begin{aligned} K_{\alpha\beta} \;=\; & \int_\Omega \left[\Phi_\alpha + \frac{\Delta t}{2} \left(\mathbf{a}_i \Phi_{\alpha,i} + \mathbf{b}_i \Phi_{\alpha,i} + \mathbf{c}_{ij} \Phi_{\alpha,ij} \right) \right] \\ & \times \left[\Phi_\beta + \frac{\Delta t}{2} \left(\mathbf{a}_k \Phi_{\beta,k} + \mathbf{b}_k \Phi_{\beta,k} + \mathbf{c}_{km} \Phi_{\beta,km} \right) \right] d\Omega \end{aligned}$$

and

$$\begin{aligned} \mathbf{F}_\alpha^n \;=\; & \int_\Omega \left[\Phi_\alpha + \frac{\Delta t}{2} \left(\mathbf{a}_i \Phi_{\alpha,i} + \mathbf{b}_i \Phi_{\alpha,i} + \mathbf{c}_{ij} \Phi_{\alpha,ij} \right) \right] \\ & \times \left[\Phi_\beta - \frac{\Delta t}{2} \left(\mathbf{a}_k \Phi_{\beta,k} + \mathbf{b}_k \Phi_{\beta,k} + \mathbf{c}_{km} \Phi_{\beta,km} \right) \right] d\Omega \mathbf{U}_\beta^n \\ & + \int_\Omega \left[\Phi_\alpha + \frac{\Delta t}{2} \left(\mathbf{a}_i \Phi_{\alpha,i} + \mathbf{b}_i \Phi_{\alpha,i} + \mathbf{c}_{ij} \Phi_{\alpha,ij} \right) \right] \mathbf{B}^n \, d\Omega \end{aligned} \tag{14.2.9}$$

As noted from (14.2.7), the test function arising from the LSM formulation resembles the GPG methods discussed in Section 13.5. The functions W_α are flowfield-dependent through the Jacobians $\mathbf{a}_i$, $\mathbf{b}_i$, and $\mathbf{c}_{ij}$. Various simplifications are available [Carey and Jiang, 1987 and others].

14.2.2 FDV-LSM FORMULATION

It is possible to use the FDV scheme for applications to LSM formulation. The advantage of FDV-LSM is to contain the time dependent terms for transient analysis. We begin with the FDV equations of the form (13.6.6):

$$\mathbf{R} = \Delta \mathbf{U}^{n+1} + \mathbf{E}_i \frac{\partial \Delta \mathbf{U}^{n+1}}{\partial x_i} + \mathbf{E}_{ij} \frac{\partial^2 \Delta \mathbf{U}^{n+1}}{\partial x_i \partial x_j} + \mathbf{Q}^n \tag{14.2.10}$$

or

$$\mathbf{R} = \left(\Phi_\alpha + \mathbf{E}_i \frac{\partial \Phi_\alpha}{\partial x_i} + \mathbf{E}_{ij} \frac{\partial^2 \Phi_\alpha}{\partial x_i \partial x_j} \right) \Delta \mathbf{U}_\alpha^{n+1} + \mathbf{Q}^n$$

The test function for the LSM scheme is

$$W_\alpha = \frac{\partial \mathbf{R}}{\partial \mathbf{U}_\alpha^{n+1}} = \Phi_\alpha + \mathbf{E}_i \Phi_{\alpha,i} + \mathbf{E}_{ij}\, \Phi_{\alpha,ij} \tag{14.2.11}$$

Substituting (14.2.10) and (14.2.11) into (14.2.3) leads to (14.2.6)

$$K_{\alpha\beta} \Delta \mathbf{U}_\beta^{n+1} = \mathbf{F}_\alpha^n$$

where

$$\begin{aligned} K_{\alpha\beta} = \int_\Omega & (\Phi_\alpha \Phi_\beta + \mathbf{E}_k \Phi_\alpha \Phi_{\beta,k} + \mathbf{E}_{km} \Phi_\alpha \Phi_{\beta,km} \\ & + \mathbf{E}_i \Phi_{\alpha,i} \Phi_\beta + \mathbf{E}_i \mathbf{E}_k \Phi_{\alpha,i} \Phi_{\beta,k} + \mathbf{E}_i \mathbf{E}_{km} \Phi_{\alpha,i} \Phi_{\beta,km} \\ & + \mathbf{E}_{ij} \Phi_{\alpha,ij} \Phi_\beta + \mathbf{E}_{ij} \mathbf{E}_k \Phi_{\alpha,ij} \Phi_{\beta,k} + \mathbf{E}_{ij} \mathbf{E}_{km} \Phi_{\alpha,ij} \Phi_{\beta,km})\, d\Omega \end{aligned} \tag{14.2.12}$$

and

$$\mathbf{F}_\alpha^n = \int_\Omega (\Phi_\alpha + \mathbf{E}_i \Phi_{\alpha,i} + \mathbf{E}_{ij}\, \Phi_{\alpha,ij})\, \mathbf{Q}^n\, d\Omega \tag{14.2.13}$$

Once again, the computational requirements for the FDV-LSM formulation are significantly greater than those of the FDV Galerkin method.

14.2.3 OPTIMAL CONTROL METHOD

The optimal control method (OCM) was applied to a highly nonlinear integrodifferential equation such as in combined mode radiative heat transfer problems [Chung and Kim, 1984; Utreja and Chung, 1989]. It resembles the standard LSM except that penalty functions are used to provide constraints.

The basic idea is to construct a cost function in the form

$$J = \frac{1}{2} \int_\Omega (R_n R_n + \lambda_{(m)} S_m S_m)\, d\Omega \tag{14.2.14}$$

where R_n represents the residual of any governing equation and $S_m^{(i)}$ denotes a constraint function which will convert a first derivative into a second derivative with λ_m being the penalty parameter (see Section 12.1.2). For example, consider a steady-state

two-dimensional Burgers equation of the form

$$R_1 = u\frac{\partial u}{\partial x} + \mathrm{v}\frac{\partial u}{\partial x} - \nu\left(\frac{\partial \overline{S}_1}{\partial x} + \frac{\partial \overline{S}_2}{\partial y}\right) = 0$$
$$R_2 = u\frac{\partial \mathrm{v}}{\partial x} + \mathrm{v}\frac{\partial \mathrm{v}}{\partial x} - \nu\left(\frac{\partial \overline{S}_3}{\partial x} + \frac{\partial \overline{S}_4}{\partial y}\right) = 0 \tag{14.2.15}$$

with

$$S_1 = \overline{S}_1 - \frac{\partial u}{\partial x} = 0$$
$$S_2 = \overline{S}_2 - \frac{\partial u}{\partial y} = 0$$
$$S_3 = \overline{S}_3 - \frac{\partial \mathrm{v}}{\partial x} = 0 \tag{14.2.16}$$
$$S_4 = \overline{S}_4 - \frac{\partial \mathrm{v}}{\partial y} = 0$$

Substituting (14.2.15) and (14.2.16) into (14.2.14) and minimizing the cost function J, we obtain

$$\delta J = \frac{\partial J}{\partial u_\alpha}\delta u_\alpha + \frac{\partial J}{\partial \mathrm{v}_\alpha}\delta \mathrm{v}_\alpha + \lambda_{(m)}\frac{\partial J}{\partial S_m}\delta S_m = 0 \tag{14.2.17}$$

Since δu_α, $\delta \mathrm{v}_\alpha$, and δS_m are arbitrary, it follows from (14.2.17) that

$$\int_\Omega \left(R_n\frac{\partial R_n}{\partial u_\alpha} + \lambda_m\frac{\partial S_m}{\partial u_\alpha}\right)d\Omega = 0$$
$$\int_\Omega \left(R_n\frac{\partial R_n}{\partial \mathrm{v}_\alpha} + \lambda_m\frac{\partial S_m}{\partial v_\alpha}\right)d\Omega = 0 \quad (n = 1, 2,\ m, r = 1, 4) \tag{14.2.18}$$
$$\int_\Omega \left(R_n\frac{\partial R_n}{\partial \overline{S}_{m\alpha}} + \lambda_r\frac{\partial S_r}{\partial \overline{S}_{m\alpha}}\right)d\Omega = 0$$

For other problems such as in combined mode radiative heat transfer where radiation source terms are to be separately calculated iteratively, the concept of penalty functions is particularly useful. Although simultaneous solutions of these equations are costly, they are quite useful for highly nonlinear problems. Applications of the OCM are demonstrated in Sections 24.3 and 24.4.

14.3 FINITE POINT METHOD (FPM)

Mesh configurations including local elements and nodal points are required for all computational methods discussed so far. In recent years, various methods which depend on finite number of points rather than meshes (meshless methods) have been developed. The so-called smooth particle hydrodynamics (SPH) [Lucy, 1977; Monaghan, 1988] has been used for the analysis of exploding stars and dust clouds using finite number of

points with a functional representation of the variable $u(x)$ as

$$u(x) = \int_{\Omega} w(x - x_i)u(x_i)\, d\Omega = \Phi_i u_i \tag{14.3.1}$$

where $w(x - x_i)$ is the kernel, wavelets, or weight function and Φ_i is the SPH interpolation function, with the kernel being approximated by exponential, cubic spline, or quartic spline.

The concept of SPH can be extended to a meshless approach in terms of element-free Galerkin method (EFG) [Belytschko et al., 1996] or fixed least squares (FLS) and moving least square (MLS) procedures [Lancaster and Salkauskas, 1981; Onate et al., 1996]. In the FLS and MLS methods, we replace the integral (14.3.1) of the variable $u(x)$ by

$$u(x) = P_i(x)a_i(x) \tag{14.3.2}$$

where $P_i(x)$ are the monomial basis functions and $a_i(x)$ are their coefficients.

$$P_i = (1, x, x^2 \ldots) \qquad \text{1D} \tag{14.3.3a}$$

$$P_i = (1, x, y, x^2, xy, y^2, \ldots.) \qquad \text{2D} \tag{14.3.3b}$$

Expanding (14.3.2) to cover nodal points, we rewrite (14.3.2) as

$$u_i = P_{ik}a_k \tag{14.3.4}$$

where

$$P_{ik} = \begin{bmatrix} P_1(x_1) & P_2(x_1) & \cdots & P_m(x_1) \\ P_1(x_2) & P_2(x_2) & \cdots & P_m(x_2) \\ \vdots & \vdots & \vdots & \vdots \\ P_1(x_n) & P_2(x_n) & \cdots & P_m(x_n) \end{bmatrix} \tag{14.3.5}$$

In order to determine the unknown coefficients $a_{i,}$, we introduce in (14.3.4) the weighted least squares operation in the form,

$$\frac{\partial J}{\partial a_i} = 0 \tag{14.3.6}$$

where J is the weighted least squares function,

$$J = W_{ij}(P_{ik}a_k - u_i)(P_{jm}a_m - u_j) \tag{14.3.7}$$

with W_{ij} being the second order tensor weight functions,

$$W_{ij} = \begin{bmatrix} W(x - x_1) & 0 & \cdots & 0 \\ 0 & W(x - x_2) & \cdots & 0 \\ \vdots & \vdots & \vdots & \vdots \\ 0 & 0 & \cdots & W(x - x_n) \end{bmatrix} \tag{14.3.8}$$

Performing the differentiation in (14.3.6) leads to

$$a_i = (W_{nj}P_{nk}P_{jm})^{-1}W_{km}P_{ir}u_r \tag{14.3.9}$$

Substituting (14.3.9) into (14.3.2), we obtain

$$u(x) = \Phi_i u_i \tag{14.3.10}$$

where Φ_i is the finite point interpolation function,

$$\Phi_i = P_s(W_{nj} P_{nk} P_{jm})^{-1} W_{km} P_{si} \tag{14.3.11}$$

with

$$\Phi_i(x_j) = \delta_{ij} \tag{14.3.12}$$

and the diagonal component of the weighting functions may be chosen as a Gaussian function

$$W_{ij} = \frac{\exp[-(x/c)^2] - \exp[-(x_m/c)^2]}{1 - \exp[-(x_m/c)^2]} \tag{14.3.13}$$

where x_m is the half size of the support and c is a parameter determining the geometrical shape.

Another meshless (finite point) method, known as the partition of unity (PUM) or *h-p* cloud method, was advanced by Duarte and Oden [1996] and Melenk and Babuska [1996], which is suitable for an unstructured adaptive method (Chapter 19). In this method, the variable $u(x)$ is expressed as

$$u(x) = \Phi_i u_{i(mnp)} \tag{14.3.14}$$

where Φ_i is the MLS function of (14.3.11) and $u_{i(mnp)}$ is the spectral function consisting of either Lagrange or Legendre polynomials with m, n, p representing orders of polynomials similarly as in (14.1.16).

The functional representation of SPH, MLS, and PUM is based on the meshless approach. Lumping them all together, these meshless methods may be called the finite point methods (FPM), as suggested by Onate et al. [1996]. The advantage of FPM is obviously the elimination of the need for grid generation, which is itself a major task.

14.4 EXAMPLE PROBLEMS

In this section, we present some example problems of FDV spectral element methods using the Legendre polynomials [Yoon and Chung, 1996]. Spectral elements of Legendre polynomial degree 2 ($q2$) in space 2 ($S2$) are applied in the spatially evolving three-dimensional boundary layers with shock wave boundary layer interactions in a single and double sharp leading edged fins.

14.4.1 SHARP FIN INDUCED SHOCK WAVE BOUNDARY LAYER INTERACTIONS

To investigate the interaction of a shock wave with a boundary layer in three dimensions, a sharp leading edged fin is adopted as a model problem. Figure 14.4.1.1a shows the physical domain for a 3-D sharp fin ($\alpha = 20^\circ$) with a general flowfield structure

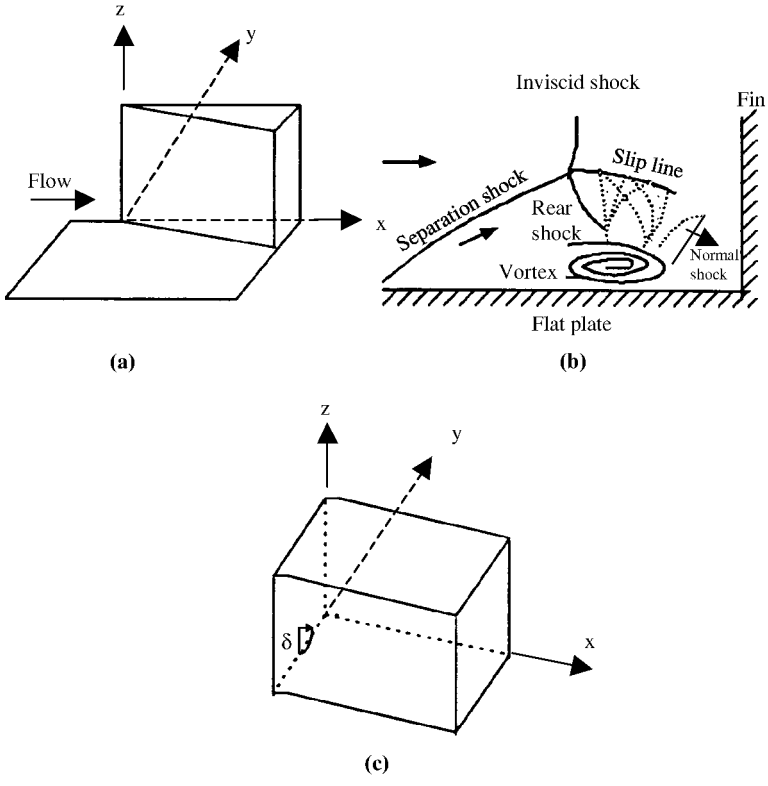

Figure 14.4.1.1 Computational domain for a 3-D 20° fin and flowfield structure with $M_\infty = 2.93$, $P_\infty = 20.57$ kPa, $T_\infty = 92.39$ K, $\mathrm{Re}_\infty = 7 \times 10^8$/m. The inlet boundary conditions are obtained from the boundary layer analysis. On the solid surface, no-slip and adiabatic wall boundary conditions are applied. **(a)** 3-D 20° fin. **(b)** 20° fin interaction flowfield structures. **(c)** Computational domain.

(Figure 14.4.1.1b) [Settles and Dolling, 1990]. The inlet boundary conditions and the corresponding flowfield structure are the same as in Knight et al. [Settles and Dolling, 1990]. Here, the freestream Mach number and temperature are $M_\infty = 2.93$ and $T_\infty = 92.39$ K, corresponding to the chamber pressure and temperature of 680 kPa and 251 K, respectively, with the Reynolds number of 7×10^8/m. The boundary layer thickness δ_o at the apex of the fin is 1.4 cm, yielding a Reynolds number $\mathrm{Re}_{\delta o} = 9.8 \times 10^5$. In order to match the boundary conditions as used for the experiments [Settles and Dolling, 1990], the flowfield behind the fin is calculated as a flat plate boundary layer such that the computed boundary layer thickness δ_o is set equal to the experimental value of 1.4 cm. On the solid surfaces, no-slip and adiabatic wall boundary conditions are applied. On the upper, lateral, and downstream exit boundaries, the flow variables are set free. Adaptive spaced grid points are 33, 41, and 31 in the streamwise, spanwise, and vertical directions, respectively. Spectral elements of Legendre polynomial degree 2 in space 2 are applied in the boundary layer.

Figure 14.4.1.2 shows the background flowfield based on the geometric configurations and boundary conditions described in Figure 14.4.1.1, as observed from the front

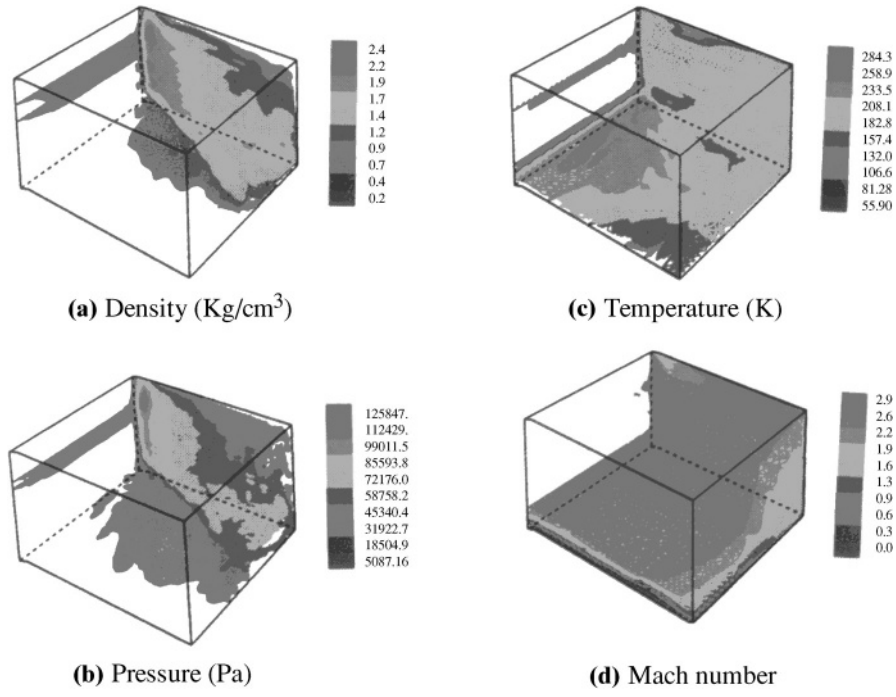

Figure 14.4.1.2 Background flowfield as observed from the front (x-z plane and y-z plane).

(x-z and y-z faces). As such, no details of the hidden portion are shown. It is noticed that the trend is in reasonable agreement with the results of Narayanswami, Hortzman, and Knight [1993], with density and pressure increasing drastically along the shock waves, the temperature rise being distributed along the flat plate, and Mach number sharply decreasing through the shock waves toward the flat plate boundary.

Vorticity variations at different planes are shown in Figures 14.4.1.3a through 14.4.1.3e. The contours of vorticity component in the streamwise planes (y-z planes) in the x-direction with each plane identified as a, b, c, d, e are shown. The corresponding velocity vectors are plotted on the right-hand side. Clearly, the vortex stretching occurs toward downstream with the evidence of separation shocks, slip lines, and vortex centers close to the wall. These physical phenomena become more significant toward downstream in agreement with the schematics shown in Figure 14.4.1.2.

Figure 14.4.1.4a shows the contours of vorticity component in the spanwise vertical planes ($x \cos \alpha$-z planes) in the $y \cos \alpha$-direction, with each plane identified as a, b, c, d. The vortex stretching occurs again toward downstream and moving upward away from the shock. The growth of vorticity is concentrated within the boundary layer close to the wall.

In Figure 14.4.1.4b, the spanwise horizontal plane vorticity contours are presented at various locations (a:$2\delta_o$, b:$2\delta_o$, c:$20.5\delta_o$) where δ_o is the boundary layer thickness. It is seen that vorticity increases toward the wall, with its intensity increasing toward downstream as expected.

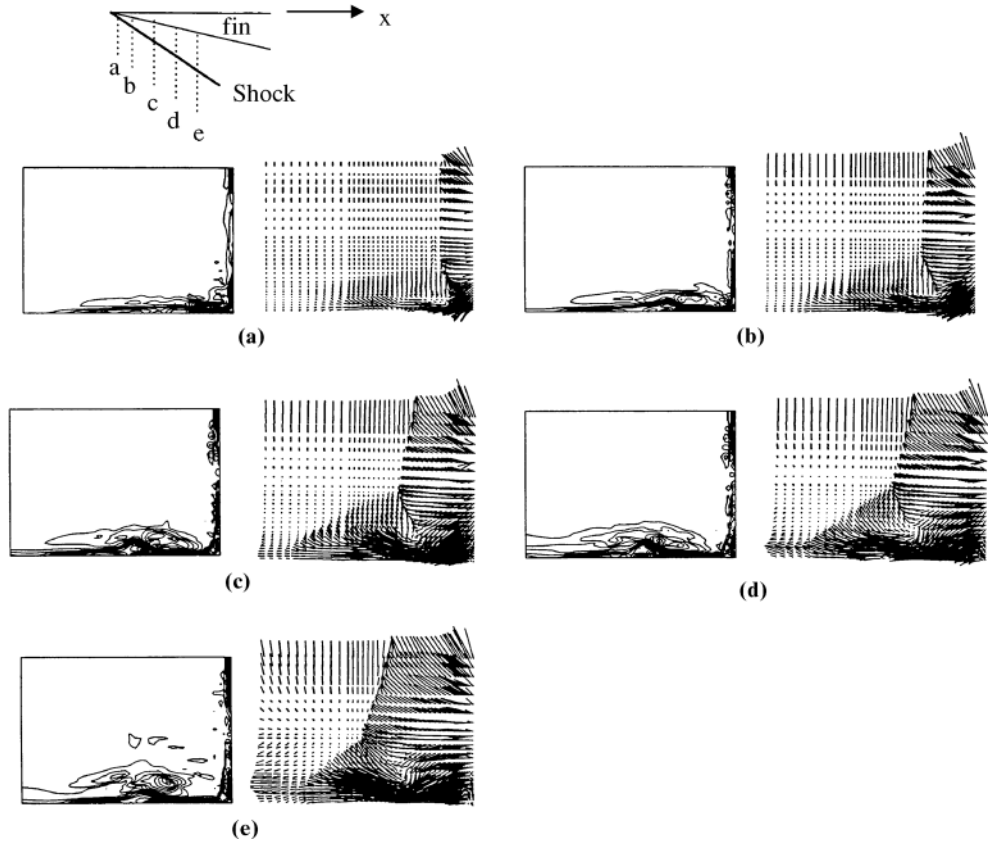

Figure 14.4.1.3 Streamwise vorticity contours and the corresponding velocity vectors ($t = 0.3965$ ms). The vortex stretching occurs toward downstream with the evidence of separation shocks, slip lines, and vortex centers close to the wall.

14.4.2 ASYMMETRIC DOUBLE FIN INDUCED SHOCK WAVE BOUNDARY LAYER INTERACTION

Complex three-dimensional shock wave boundary layer interactions occur on asymmetric double fins. Schematic representation of an asymmetric crossing shock wave turbulent boundary layer interaction is shown in Figure 14.4.2.1a. The dimensions and freestream conditions employed in the experiment by Knight et al. [1995] are shown in Figure 14.4.2.1b. The same dimensions and freestream conditions are used in the present investigation.

Figures 14.4.2.2a and 14.4.2.2b display density and pressure contours, respectively. Existence of crossing shock waves and expansion waves in the asymmetric double fins is clearly evident in these figures. Figure 14.4.2.3 shows velocity vectors at different streamwise planes (y-z planes) in the x-direction. It is evident that vortices are generated near the surface toward downstream.

The present result is compared with experimental data [Knight et al., 1995] for wall pressure. The comparisons on the throat middle line and at streamwise location

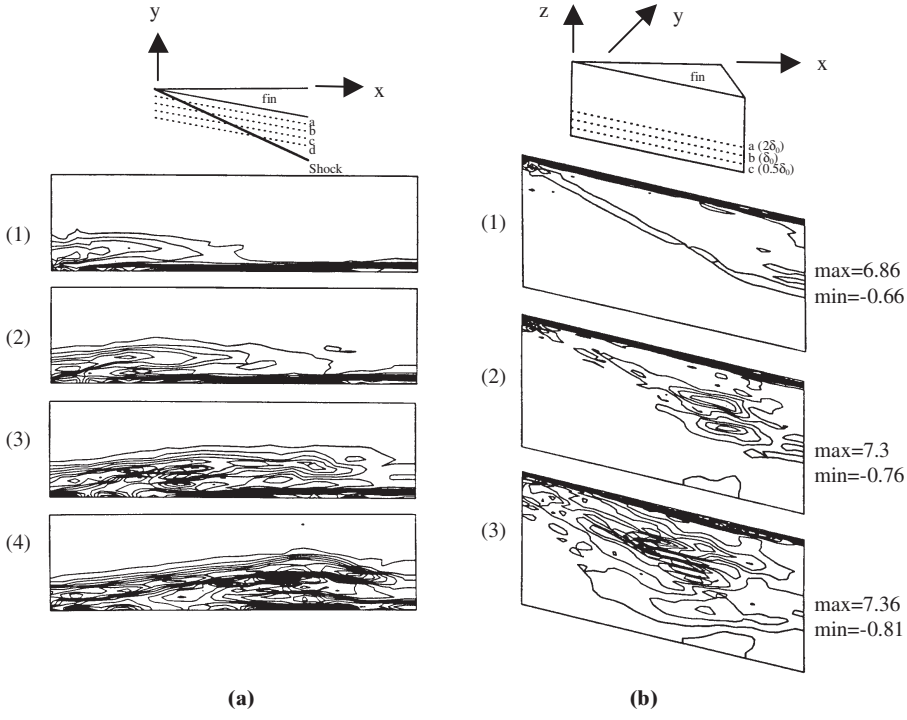

Figure 14.4.1.4 Spanwise vertical and horizontal plane vorticity contours. **(a)** Spanwise vertical plane ($x\cos\alpha$-z plane) vorticity contours at various locations ($t = 0.3965$ ms, $0 \le z/\delta_0 \le 2.5$). The vortex stretching occurs again toward downstream and moving upward away from the shock. The growth of vorticity is concentrated within the boundary layer close to the wall. **(b)** Spanwise horizontal plane ($x\cos\alpha$-y plane) vorticity contours at various locations ($t = 0.3965$ ms). Is is seen that vorticity increases toward the wall with its intensity increasing toward downstream as expected.

$x = 46$ mm are displayed in Figure 14.4.2.4a and Figure 14.4.2.4b, respectively. The present and experimental surface pressure on throat middle line are in general agreement at upstream, but deviate toward downstream. At $x = 46$ mm, the present and experimental surface pressures show a close agreement.

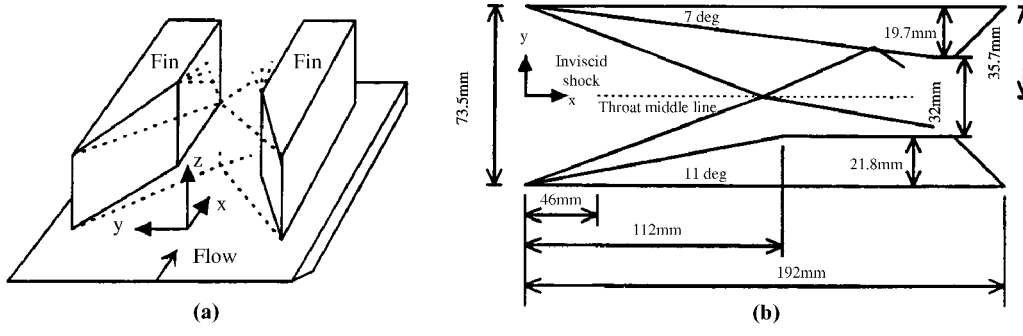

Figure 14.4.2.1 Asymmetric double fin induced shock wave boundary layer interactions. **(a)** Schematic representation of asymmetric crossing shock wave turbulent boundary layer interaction. **(b)** Asymmetric double fins with $M_\infty = 3.85$, $Re_{\delta\infty} = 3 \times 10^5$, $P_t = 1.5$ MPa, $T_t = 270$ K, $\delta_\infty = 3.5$ mm.

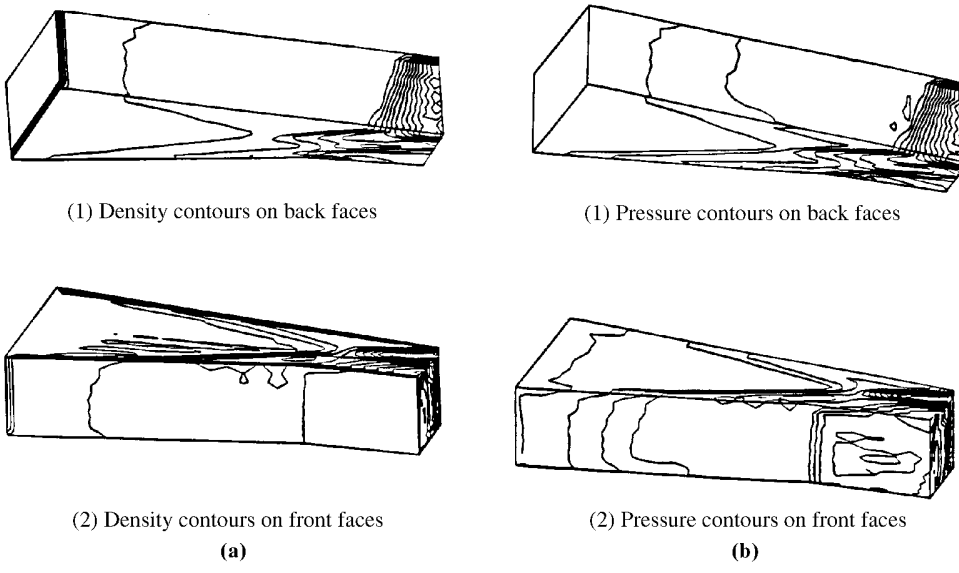

Figure 14.4.2.2 Density and pressure distributions. **(a)** Density contours (min = 0.6 kg /m^3, max = 2.3 kg/ m^3), existence of crossing shock waves and expansion waves appears. **(b)** Pressure contours (min = 11 kPa, max-79 kPa).

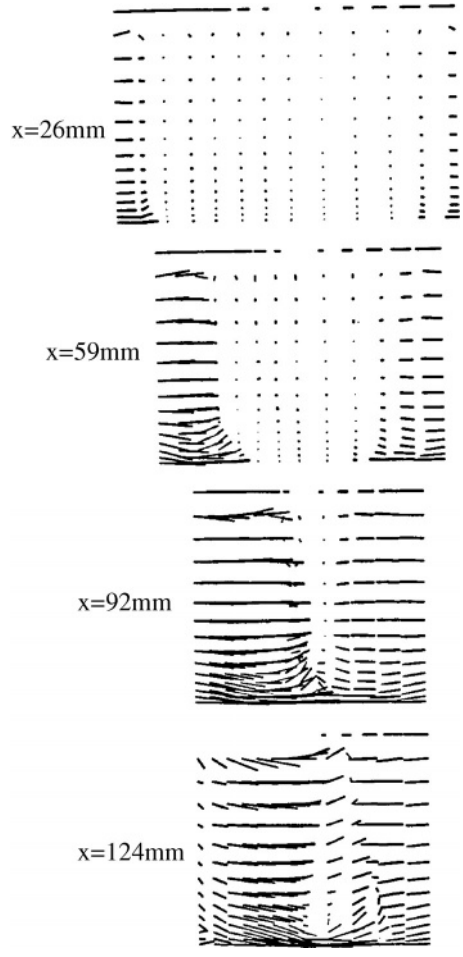

Figure 14.4.2.3 Velocity vectors at different streamwise stations. Vortices are generated near the surface toward downstream.

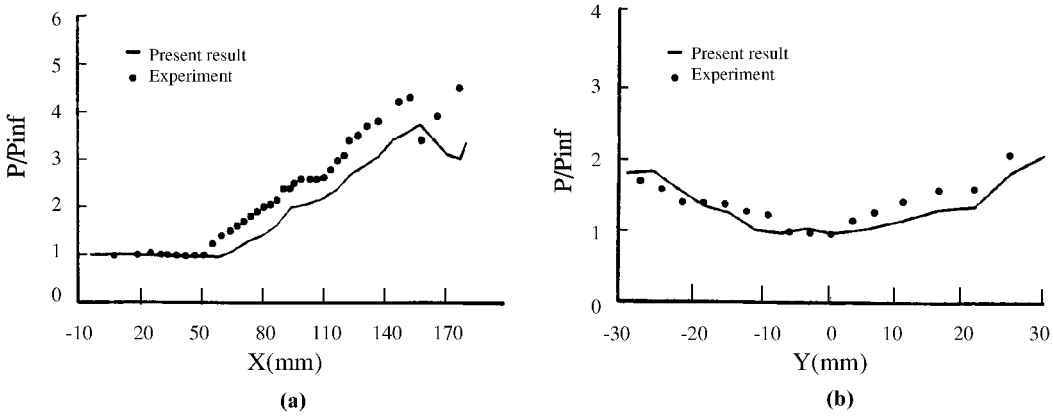

Figure 14.4.2.4 Comparison of pressure distributions with experimental data. **(a)** Comparison between the present result and experimental data of wall pressure on throat middle line. The present and experimental surface pressures on throat middle line are in general agreement at upstream, but deviate toward downstream. **(b)** Comparison of wall pressure at $x = 46$ mm for the present result and experimental data. At $x = 46$ mm, the present and experimental surface pressure show close agreement.

14.5 SUMMARY

In this chapter, we reviewed various methods that are related to FEM or weighted residual methods. Although the spectral element methods (SEM) are accurate for simple geometries and simple boundary conditions, the SEM applications to complex multidimensional problems are not practical. The least squares methods (LSM) can be applied to complicated geometries, but computations involved are quite time-consuming. The research in meshless methods or finite point methods (FPM) has begun recently. Active research in FPM in the future appears to be promising.

As we come to the end of finite element applications, we recall that, in Part Two, the finite volume methods (FVM) can be formulated using FDM as shown in Chapter 7. Thus, a similar treatment of FVM using FEM is the subject of the next chapter.

REFERENCES

Babuska, I. [1958]. The *p* and *h-p* versions of the finite element method. The state of the art. In D. L. Dwoyer, M. Y. Hussaini, and R. G. Voigt (eds.). *Finite Elements Theory and Application*, 199–239, New York: Springer-Verlag.

Belytschko, T., Krongauz, Y., Organ, D., Fleming, M., and Krysl, P. [1996]. Meshless methods: An overview and recent developments. *Comp. Meth. Appl. Mech. Eng.*, 139, 3–47.

Bramble, J. H. and Shatz, A. H. [1970]. On the numerical solution of elliptic boundary-value problems by least-squares approximation of the data. In B. Hubbered (ed.). *Numerical Solution of PDE, Vol. 2*, New York: Academic Press.

Canuto, C., Hussani, M. Y., Quarteroni, A., and Zang, T. A. [1987]. *Spectral Methods in Fluid Dynamics*. New York: Springer-Verlag.

Carey, G. F. and Jiang, B. N. [1987]. Least squares finite element method and preconditioned conjugate gradient solution. *Int. J. Num. Meth. Eng.*, 24, 1283–96.

Chung, T. J. and Kim, J. Y. [1984]. Two-dimensional, combined-mode heat transfer by conduction, convection and radiation in emitting, absorbing and scattering media – solution by finite elements. *J. Heat Trans.*, 106, 448–52.

Duarte, C. A. and Oden, J. T. [1996]. An *hp* adaptive method using clouds. *Comp. Meth. Appl. Mech. Eng*., 139, 237–62.

Fix, G. J. and Gunzburger, M. D. [1978]. On the least squares approximations to indefinite problems of the mixed type. *Int. J. Num. Meth. Eng.* 12, 453–69.

Knight, D. D., Garrison, T. J., Senles, G. S., Zheltovodov, A. A., Maksimov, A. I., Shevehenko, A. M., and Vorontsov, S. S. [1995]. Asymmetric crossing-shock-wave/turbulent-boundary-layer interaction. *AIAA J.*, 33, 12, 2241.

Lancaster, P. and Salkauskas, K. [1981]. Surfaces generated by moving least squares methods. *Math. Comp.*, 37, 141–58.

Lucy, L. B. [1977]. A numerical approach to the testing of the fission hyporthesis. *Astron. J.*, 8, 12, 1013–24.

Lynn, P. P. [1974]. Least squares finite element analysis of laminar boundary layer flows, *Int. J. Num. Meth. Eng*., 8, 865–76.

Melenk, J. M. and Babuska, I. [1996]. The partition of unity finite element method. *Comp. Meth. Appl. Mech. Eng*., 139, 289–314.

Monaghan, J. J. [1988]. An introduction to SPH. *Comp. Phys. Comm*., 48, 89–96.

Narayanswami, N., Hortzman, C. C., and Knight, D. D. [1993]. Computation of crossing shock/turbulence layer interaction at Mach 8.3. *AIAA J*., 31, 1369–76.

Oden, J., Demkowicz, L., Rachowicz, W., and Westermann, T. A. [1989]. Toward a universal *h-p* adaptive finite element strategy: Part II. A posteriori error estimation. *Comp. Meth. Appl. Mech. Eng.*, 77, 113–80.

Onate, E., Idelsohn, S., Zienkiewicz, O. C., Taylor, R. L., and Sacco, C. [1996]. A stabilized finite point method for analysis of fluid mechanics problem. *Comp. Meth. Appl. Mech. Eng*., 139, 315–46.

Patera, A. T. [1984]. A spectral method for fluid dynamics, laminar flow in a channel expansion. *J. Comp. Phys.*, 54, 468–88.

Settles, G. S. and Dolling, D. S. [1990]. Swept shock/boundary-layer interactions: Tutorial and update. *AIAA* 90–0375.

Sherwin, S. J. and Karniadakis, G. E. [1995]. A triangular spectral element methods; applications to the incompressible Navier-Stokes equations. *Comp. Meth. Appl. Mech. Eng.,* 123, 189–229.

Szabo, B. A. and Babuska, I. [1991]. *Finite Element Analysis*. New York: Wiley.

Utreja, L. R. and Chung, T. J. [1989]. Combined convection-conduction-radiation boundary layer flows using optimal control penalty finite elements. *J. Heat Trans.*, 111, 433–37.

Yoon, K. T. and Chung, T. J. [1996]. Three-dimensional mixed explicit-inplicit generalized Galerkin spectral element methods for high-speed turbulent compressible flows. *Comp. Meth. Appl. Mech. Eng*., 135, 343–67.